Journal of Cellular Physiology

Human Monocyte-Derived Macrophages Spontaneously Differentiated In Vitro Show Distinct Phenotypes

SONIA ELIGINI,[1]* MAURO CRISCI,[1] ELISA BONO,[1] PAOLA SONGIA,[1] ELENA TREMOLI,[1,2] GUALTIERO I. COLOMBO,[1] AND SUSANNA COLLI[2]

[1]*Centro Cardiologico Monzino, IRCCS, Milano, Italy*

[2]*Dipartimento di Scienze Farmacologiche e Biomolecolari, Università degli Studi di Milano, Milano, Italy*

Tissue macrophages are resident phagocytes that acquire specific phenotypes according to the microenvironment. Morphological and functional heterogeneity has been evidenced in different homeostatic and pathological conditions. Indeed, the nature of macrophage subsets may have either harmful or beneficial functions in disease progression/resolution. Therefore the possibility to pharmacologically manipulate heterogeneity represents a relevant challenge. Since human tissue macrophages are not easily obtained, various in vitro models are currently used that do not adequately reflect the heterogeneity and plasticity of tissue macrophages. We had previously reported that two dominant and distinct macrophage morphotypes co-exist in the same culture of human monocytes spontaneously differentiated for 7 days in autologous serum. The present study was aimed to the phenotypic characterization of these morphotypes, that is, round- and spindle-shaped. We observed that, besides substantial differences in cytoskeleton architecture, round monocyte-derived macrophages (MDMs) showed higher lipid content, increased macropinocytosis/efferocytosis capacity, and overexpression of CD163, interleukin (IL)-10, and transforming growth factor (TGF) β2. Conversely, spindle MDMs exhibited enhanced respiratory burst and higher expression of the chemokine (C-C motif) ligands 18 and 24 (CCL18 and CCL24). Overall, round MDMs show functional traits reminiscent of the non-inflammatory and reparative M2 phenotype, whereas spindle MDMs exhibit a pro-inflammatory profile and express genes driving lymphocyte activation and eosinophil recruitment. MDMs obtained in the culture condition herein described represent a valuable model to disentangle and manipulate the functional heterogeneity of tissue macrophages that has been disclosed in scenarios spanning from inflammatory and wounding responses to atherosclerotic lesions.

J. Cell. Physiol. 228: 1464–1472, 2013.

Differentiated tissue macrophages develop both from blood-derived monocytes (Gordon and Taylor, 2005) and from tissue resident progenitors (Ley et al., 2011). Upon differentiation, macrophages become resident and acquire specific functions according to the characteristics of tissue microenvironment that mould their behavior (Lambrecht, 2006; Lumeng et al., 2007). Key macrophage functions are aimed at maintaining tissue homeostasis: they include phagocytosis and killing of invading pathogens, release of mediators of inflammation and healing, antigen presentation and processing. Macrophages are heterogeneous in phenotype, a feature due to an intrinsic differentiation program that results in morphologic and functional differences (Mosser and Edwards, 2008). In addition, exogenous stimuli, either microbial or environmental, affect the phenotype (Benoit et al., 2008). Macrophage heterogeneity has been evidenced in different homeostatic and pathological settings that span from wound healing (Sindrilaru et al., 2011) to autoimmunity (Murray and Wynn, 2011), tumor progression (Mantovani et al., 2002), and atherosclerotic lesions (Johnson and Newby, 2009). In particular, in this latter scenario, macrophage populations, distinct for morphology, functional properties and genomic signatures, may direct plaque progression and rupture, with important implications for therapy (Wilson, 2010). Emerging data, indeed, raise the possibility to pharmacologically manipulate macrophage functions (Fujita et al., 2010).

Tissue macrophages, however, are not easily obtained and handled without affecting viability. Monocytic cell lines exposed to differentiating agents exhibit important differences when compared with primary tissue macrophages or with macrophages differentiated in vitro from blood-derived monocytes (Daigneault et al., 2010) and, above all, they do not adequately address the crucial issue of heterogeneity. Monocyte-derived macrophages (MDMs) are commonly accepted as a good surrogate of macrophages infiltrating tissues. Distinct phenotypes are currently obtained upon monocyte exposure to bacterial agents, cytokine/chemokine cocktails (Mantovani et al., 2004), or colony stimulating factors (CSFs; Akagawa, 2002), allowing the functional dissection of MDMs into classically (M1) or alternatively (M2) activated, which are respectively associated with inflammatory and tissue reparative responses. Nevertheless, these experimental polarizations might not adequately reflect the features and plasticity of un-manipulated tissue macrophages.

A previous study from our group provided evidence that two dominant MDM subsets, distinguishable for morphology (round- or spindle-shaped), co-exist in the same culture of blood-derived monocytes spontaneously differentiated in vitro in autologous serum (Colli et al., 1999). We report here that

Conflict of interest: none.

Contract grant sponsor: Università degli Studi di Milano (to S.C.); Contract grant number: PUR 2009-ATE-0179.

*Correspondence to: Sonia Eligini, Centro Cardiologico Monzino, IRCCS, via Parea 4, 20138, Milano, Italy.
E-mail: sonia.eligini@cardiologicomonzino.it

Manuscript Received: 3 September 2012
Manuscript Accepted: 27 November 2012

Accepted manuscript online in Wiley Online Library (wileyonlinelibrary.com): 18 December 2012.
DOI: 10.1002/jcp.24301

the distinct MDM morphotypes exhibit different antigenic and functional profiles. This model may be useful to focus on macrophage heterogeneity, a feature that has been disclosed in settings spanning from the inflammatory and wounding response to the atherosclerotic lesion.

Materials and Methods

Monocyte isolation and culture

Monocytes were isolated from venous blood of healthy consenting volunteers, after Local Research Ethics Committee approval. The study was conducted according to the principles expressed in the Declaration of Helsinki. Blood samples whose white cell count was not within the normal range were not processed. Mononuclear cells were isolated by Ficoll-Paque Plus (GE Healthcare, vWR Int., Milan, Italy) density centrifugation at 450g for 20 min at room temperature. To remove platelet contamination, lymphocyte/monocyte-rich layer was washed with PBS containing 5 mM EDTA and suspended in RPMI 1640 (Lonza Milano S.r.l, Bergamo, Italy) supplemented with 2 mM L-glutamine (Lonza), 100 U/ml penicillin, 100 μg/ml streptomycin (Lonza), and 10% autologous serum freshly obtained from blood clotted for 2 h at 37°C. Mononuclear cells were then plated (2×10^6/ml) in 35 mm well plates (Primaria™, Falcon, Sacco S.r.l, Como, Italy) or, for laser capture microdissection (LCM) experiments, in DuplexDish 50 (Carl Zeiss S.p.A, Milan, Italy) and kept at 37°C (5% CO_2). After 90 min, non-adherent cells were removed and those adherent were cultured over 7 days at 37°C (5% CO_2) in Medium 199 (Lonza) supplemented with 2 mM L-glutamine, 100 U/ml penicillin, 100 μg/ml streptomycin, and 10% autologous serum. Medium was not replaced throughout the culture period. The mean cell protein content increased with monocyte differentiation from 5–15 to 70–300 μg/ml. The endotoxin levels of all culture materials and reagents used was measured by the Limulus amoebocyte lysate assay (Lonza). To avoid MDM activation, only preparations free of endotoxin or containing <30 pg/ml were used.

Flow cytometry

Adhered monocytes (90 min-adhesion) and MDMs were detached and analyzed by FACSCalibur (BD Biosciences, Milan, Italy). Forward and side scatter light was used to identify cell populations and to measure size and granularity of monocytes and MDMs. For detection of MDM cell surface markers, samples containing 1×10^6 cells were incubated with monoclonal mouse anti-human antibodies CD45 APC-H7, CD3 APC, CD19 PE, CD56 PE, CD34 FITC, CD83 FITC, or isotype-matched irrelevant antibodies (BD Biosciences) for 15 min at room temperature. Samples were then washed, suspended in PBS and 10,000/sample events for each marker were recorded. All data were analyzed using CellQuest™ Pro software (BD Biosciences).

Fluorescence

Adhered MDMs were fixed (2% para-formaldehyde, PFA, for 20 min at room temperature) and non-specific reactive sites were blocked with 5% bovine serum albumin (BSA) solution containing 0.1% saponin (30 min, room temperature). MDMs were incubated overnight at 4°C with monoclonal mouse anti-human antibodies directed toward CD68 and interleukin (IL)-10 (Abcam, Prodotti Gianni S.p.A., Milan, Italy), von Willebrand factor (Dako Italia, S.p.A., Milan, Italy), late stage inflammatory antigen 25F9 (Chemicon, Millipore S.p.A., Milan, Italy), acetylated α- and β-tubulin (Serotec, Space Import-Export S.r.l, Milan, Italy), and CD163 (Serotec). F-actin was assessed by phalloidin^{TRITC} (Sigma–Aldrich, Milan, Italy) staining (32 μg/ml, 1 h, room temperature). Detection was performed with appropriate Alexa Fluor 488 (green emission) or 594 (red emission) conjugated secondary antibodies (10 μg/ml, 60 min, room temperature) (Life Technologies Italia, Monza, Italy). Negative control experiments were performed by omitting the primary antibodies.

MDM lipid content was assessed using the lipophilic dye Nile Red (Sigma–Aldrich). For this purpose, living MDMs were incubated with the staining solution (0.1 mg/ml) for 15 min at room temperature and fluorescence was detected at 605 nm.

The intracellular production of superoxide was evaluated in MDMs either resting or exposed to phorbol myristate acetate, PMA (Sigma–Aldrich) (40 nM, 2 h). Dihydroetidium (DHE, Life Technologies Italia) was added (10 μM concentration) 20 min before the end of incubation to allow the oxidation of DHE to a red fluorescent product, which intercalates with DNA (Zielonka et al., 2008). Fluorescence was detected at 605 nm.

Lectin-mediated endocytosis and macropinocytosis were assessed using 1 mg/ml of Dextran^{FITC} 40 kDa (Sigma–Aldrich) and Lucifer Yellow dipotassium salt (Sigma–Aldrich), respectively. MDMs were incubated for 2 h at 37°C in M199. At the end of incubation, cells were washed and fixed with 2% PFA for 20 min at room temperature.

To assess binding/uptake of apoptotic cells, Jurkat T-cells (2×10^6/ml) were labelled with 5 μM carboxy fluorescein diacetate succinimidyl ester (CFSE, Life Technologies Italia) for 30 min at 37°C before the induction of apoptosis. CSFE-labeled apoptotic cells were co-cultured with MDMs (2:1 ratio) for different time frames. Non-ingested apoptotic cells were removed. Data are expressed as the percentage of MDMs that have bound/engulfed fluorescent apoptotic cells, reported to the total macrophage morphotype. In all experiments nuclei were stained with 1 μg/ml Hoechst 33258 (Sigma–Aldrich) for 10 min at room temperature.

Cytochemistry

After fixation MDMs were permeabilized and non-specific reactive sites were blocked with 5% BSA solution containing 0.1% saponin for 30 min at room temperature and incubated with anti-myeloperoxidase antibody (Dako) for another 30 min at room temperature. After three washings, cells were incubated with biotinylated secondary antibody (Dako) for 30 min at room temperature and subsequently incubated with alkaline phosphatase conjugated streptavidin (Life Technologies Italia) for 30 min to visualize immune complexes. Nuclei were counterstained with Meyer's hemalum solution.

Intracellular production of superoxide was evaluated in resting MDMs exposed to 0.8 mg/ml nitroblue tetrazolium (NBT, Sigma–Aldrich). Incubations (37°C) lasted 20 min at room temperature, to allow the reduction of NBT to formazan. Intracellular formazan was visualized by phase contrast microscopy (AxioSkop 2 plus, Zeiss) as blue/violet crystals (Sutherland and Learmonth, 1997).

Apoptosis of Jurkat T-cells

Jurkat T-cell line, clone E6-1 (ATCC), was purchased from LGC Standards S.r.l., Milan, Italy, and cultured in RPMI 1640 supplemented with 10% fetal calf serum (Lonza) and 26 mM HEPES. Early and late apoptotic Jurkat cells were obtained upon incubation (4×10^6 cells/ml) in serum-free RPMI 1640 with 10 μM etoposide (Sigma–Aldrich) for 2 and 20 h, respectively. The extent of apoptosis was evaluated by flow cytometry using annexin V PE (BD Biosciences), according to the manufacturer's instructions. A total of 20,000/sample events were acquired. Apoptosis was also assessed in PFA-fixed Jurkat T-cells by the evaluation of chromatin condensation (Hoechst 33258 stain, Sigma–Aldrich).

Quantitative image analysis

Fluorescent images were captured on an AxioObserver.Z1 microscope connected to a digital camera using the image processor AxioVision 4.7 (Carl Zeiss). Fluorescence/color intensity (densitometric sum of gray) was quantified, as an index of the amount of the molecule under study. Data are expressed as the mean level of fluorescence intensity (total intensity/number of

examined cells) for each MDM morphotype per field, subtracted of the negative control value obtained in the absence of primary antibody. Multiple fields of view (at least three fields, 400× magnification) were captured for each culture and approximately 150 cells/morphotype were analyzed. Means derive from ≥3 independent cultures obtained from different donors.

Laser capture microscopy

Co-existence of MDM morphotypes in the same culture was maintained (either quantitatively or qualitatively) also when monocytes were differentiated in DuplexDish 50 (Carl Zeiss). LCM was performed on MDM cultures obtained from six different donors using a PALM MicroLaser system (Bernried, Germany). The system is coupled via epifluorescence path with an inverted light-microscope (AxioVert 200M, Carl Zeiss) and focused through a 40× dry objective lens. MDMs were cut and captured using RoboPC autocatapulting tool. Cut elements were catapulted directly into a cup of 0.65 ml microcentrifuge tube. Approximately 150 laser-pulsed cells for each morphotype were separately collected from each culture dish.

RNA extraction and amplification

Total RNA extraction was performed using the Agencourt RNAdvance Cell v2 kit (Beckman Coulter, Milan, Italy). Briefly, cells collected into LCM cups filled with lysis buffer were spinned into a microcentrifuge tube and incubated in lysis/proteinase K solution for 30 min at room temperature. Samples were added with binding buffer containing paramagnetic beads and incubated 5 min at room temperature, to let RNA bind to the beads. Samples were placed on a magnet and washed. To eliminate genomic DNA contamination, RNA samples were treated with RNase-free Turbo DNase (Life Technologies Italia) for 15 min at room temperature. RNA was re-bind to beads and DNase was removed. Total RNA was finally eluted, precipitated in absolute ethanol added with glycogen for 1 h at −80°C, and resuspended in RNase-free H_2O. RNA integrity and quantity was assessed by capillary electrophoresis using RNA 6000 Pico Chips on a 2100 Bioanalyzer (Agilent Technologies, Milan, Italy). Extractions yielded 1.2–4.5 ng of total RNA/MDM culture. RNA was linearly amplified according to Eberwine's protocol (Van Gelder et al., 1990) in two subsequent cycles, using the MessageAmp II aRNA Amplification kit (Life Technologies Italia) following the manufacturer's instructions. At the end of every cycle, the quality and quantity of the amplified RNA (aRNA) were assessed by electrophoretic and spectrophotometric analysis.

Gene expression profiling and quantitative reverse transcription (RT)-PCR

One microgram aRNA were reverse-transcribed in 20 μl reaction using the First Strand Kit (Qiagen S.p.A., Milan, Italy), following the manufacturer's instruction. Real-Time PCR assays were set up using the 2× SABiosciences RT^2 qPCR Master Mix and a RT^2 Profiler PCR Array (Qiagen), following the manufacturer's instructions. Cytokine expression profile in each MDM preparation was investigated using the Human Cytokines & Chemokines RT^2 Profiler PCR Array. RT^2 Profiler PCR Arrays were run on a ViiA 7 Real-Time PCR system and analyzed using the ViiA 7 software v1.2 (Life Technologies Italia). For proper comparison each MDM pair was run on the same array and all the arrays were analyzed together using the Gene Expression Study tool of the ViiA 7 software. Optimal baseline and C_t were determined automatically by the software algorithm for each amplification curve. All C_t values reported as greater than 35 or as not detected were changed to 35 and considered a negative call. Three sets of replicate control wells (genomic DNA, reverse transcription, and positive PCR controls) were used to assess each groups' level of genomic DNA contamination, reverse transcription efficiency, and PCR reproducibility, as well as to test for inter-well and intra-plate consistency. Raw expression intensities of target mRNAs were normalized for differences in the amount of total RNA added to each reaction using a set of five reference genes (β-actin, ACTB; β-2-microglobulin, B2M; glyceraldehyde-3-phosphate dehydrogenase, GAPDH; hypoxanthine phosphoribosyltransferase 1, HPRT1 and ribosomal protein L13a, RPL13A). Analysis of gene expression stability and selection of the best reference genes were performed using the NormFinder version 0.953 Excel Add-In (Andersen et al., 2004). Relative quantitation of gene expression was performed using the comparative C_t method ($\triangle C_t$). $\triangle C_t$ value was defined as the difference between the C_t of a gene (either target or housekeeping) in the calibrator sample (the sample with the highest expression, i.e., lowest C_t value) and the C_t of the same gene in experimental sample. The C_t values were transformed to raw, not-normalized quantities using the formula $\eta^{\Delta Ct}$, where amplification efficiency (η) was set arbitrarily to 2 (100%). Gene expression normalization factors were obtained calculating the geometric mean of the raw quantities of the two most stable reference genes (RPL13A and ACTB). The normalized expression of each target mRNA was finally calculated by dividing the raw gene-of-interest quantity by the appropriate normalization factor.

Statistical analysis

Statistical evaluation was performed using SigmaStat software v2.03 (Jandel, San Rafael, CA). All data are expressed as mean ± standard deviation of the mean (SD). Paired-group comparison was performed using the paired *t*-test. Grouped differences were compared using two-way repeated measures ANOVA and Tukey test. Differences at $P < 0.05$ were considered statistically significant.

The MultiExperiment Viewer (MeV) software v4.8.1 (Saeed et al., 2006) was used for statistical analysis of the PCR arrays. Genes were deemed as non informative and filtered out from all plates when the percent of negative calls exceeded 30% in either morphotypes. Normalized gene expression values were log transformed ($\log_2$) and differentially expressed genes were identified using a multivariate paired *t*-test, computing *P* values based on all available sample permutations (64) with a confidence level of 95% ($1-\alpha$) and limiting the false discovery rate (FDR) proportion to <0.2. Differences in gene expression were considered statistically significant if their *P*-value was less than 0.05. Unsupervised hierarchical cluster analysis was performed to assess the similarity and differences in gene expression profiles among the samples and whether differential profile discriminates the two morphotypes. The similarity of gene expression among arrays and probes was assessed by calculating the uncentered Pearson's correlation coefficient. Normalized $\log_2$ transformed expression values were median centered and clustered by correlation average linkage, using leaf order optimization.

Results

Morphological characterization and antigenic profile of blood-derived monocytes spontaneously differentiated into macrophages

Macrophages originated from adherent monocytes cultured for 7 days showed, as expected, a cytoplasmatic volume larger than monocytes adhered for 90 min (Fig. 1A). This feature was coupled with an increased granularity, as evidenced by the augment in side scatter (SSC) on flow cytometry, possibly due to an increase of cytoplasmic organelles (Fig. 1B). A minor population of lymphocytes was also present in MDM cultures ($CD3^+$ cells 9.02 ± 6.84%; $CD19^+$ cells 3.5 ± 1.17%; $CD56^+$ cells 2.24 ± 2.29%, n = 5, from separate donors).

MDMs showed a lower myeloperoxidase (MPO) activity with respect to 2 h adhered monocytes (5.3 ± 2.1% vs. 51.8 ± 13.1% positive cells, respectively). The analysis of macrophage morphology showed mainly two dominant and distinct morphotypes that occurred in all cultures (n = 20, from

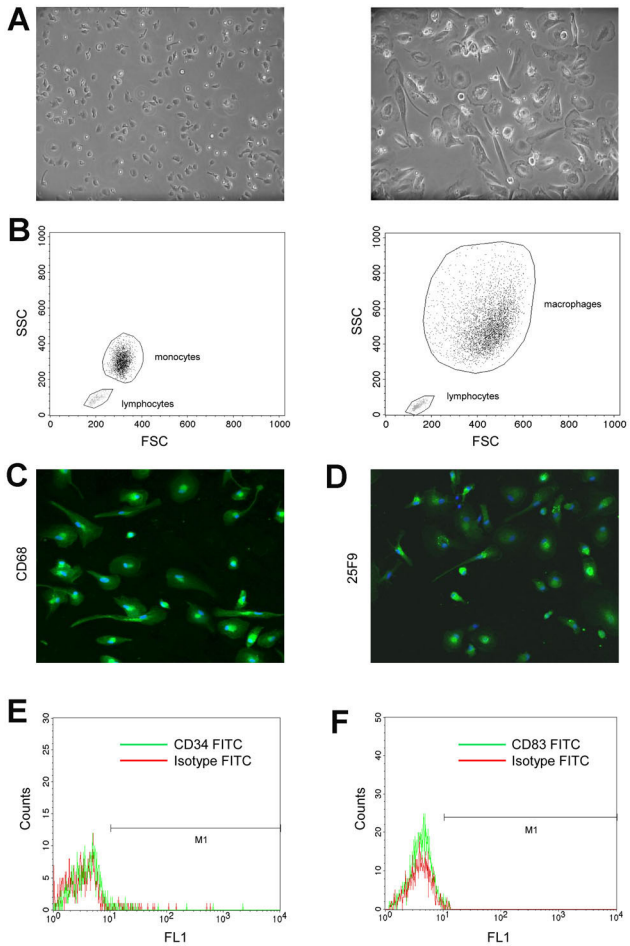

Fig. 1. Morphological changes of monocytes upon differentiation and expression of macrophage markers. Representative contrast images (AxioVert 200 M, Zeiss, 200× original magnification) of monocytes adhered for 90 min (A, left) and differentiated toward macrophages (MDMs) for 7 days in M199 supplemented with 10% autologous serum (A, right). Flow-cytometry dot plots show forward scatter (FSC) and side scatter (SSC) of monocytes, MDMs and lymphocytes (B). MDM expression of macrophage antigen CD68 (C) and tissue macrophage marker 25F9 (D) was detected by immunofluorescence (200× original magnification); nuclei (blue) are visualized by Hoechst 33258. Representative cytometric histograms show that MDMs are negative for the expression of CD34 (E) and CD83 (F), markers of fibrocytes and dendritic cells, respectively (200× original magnification, both). M1 region delimits the area of positive cells. All images are presented for at least three independent experiments from separate donors.

separate donors). Spindle/elongated (length >70 μm, width <30 μm) and round, "egg-fried," (width and length >35–40 μm) shaped cells were detected with similar frequency (38 ± 4.5% and 37 ± 6.2%, respectively). Cells, whose morphology and dimension did not satisfy the above criteria accounted for 25 ± 7.6%. Both morphotypes stained positively for the pan-leukocyte antigen CD45 (data not shown) and for the specific macrophage marker CD68 (Fig. 1C). Of interest, irrespectively from the morphotype, approximately 50% of MDMs were positive for the antigen 25F9 that characterizes mature tissue macrophages (Zwadlo et al., 1985; Fig. 1D). All cultures were negative for the antigens CD34 (Fig. 1E), CD83 (Fig. 1F) and for von Willebrand factor (not shown), which are markers of fibrocytes, dendritic cells, and endothelial cells, respectively.

Cytoskeleton architecture and lipid content

The distribution of F-actin, visualized by phalloidin staining, revealed strong qualitative and quantitative differences between the morphotypes. Round MDMs showed significantly higher F-actin labeling (Fig. 2A), which was quite regularly arranged to form a ring within the cell. In contrast, spindle MDMs showed a peculiar F-actin distribution mainly localized at the leading edge. Conversely, β-tubulin fluorescence intensity did not differ between the two morphotypes (Fig. 2B). Instead, the level of acetylated α-tubulin, a marker of stable microtubule population (Westermann and Weber, 2003), was clearly higher in round MDM, which showed a perinuclear staining (Fig. 2C).

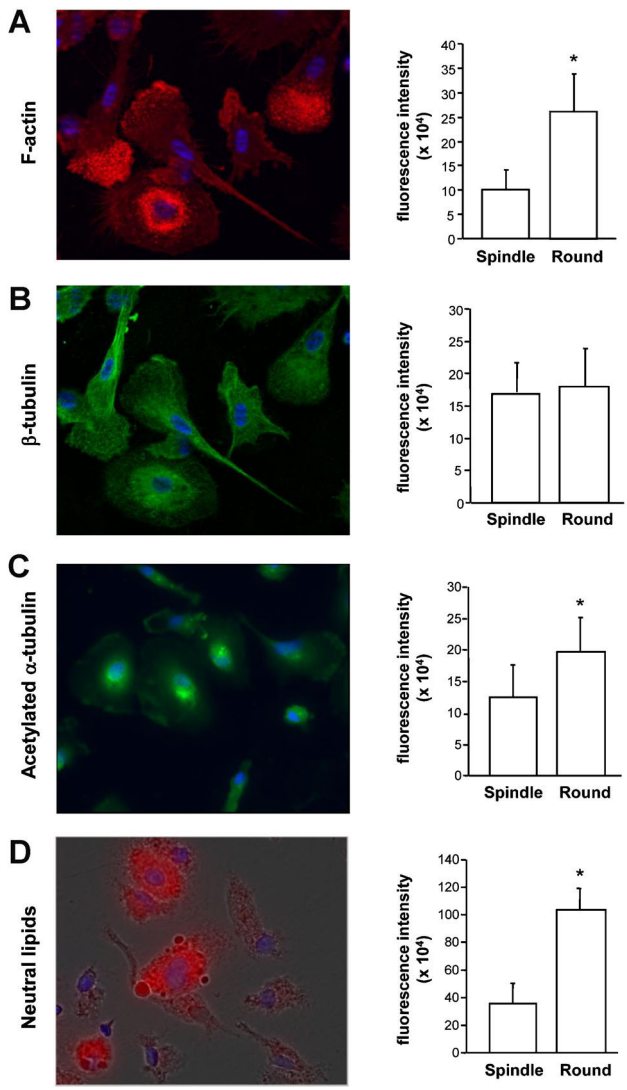

Fig. 2. Cytoskeleton architecture and lipid content. Representative images (400× magnification) and quantitative image analyses (densitometric sum of gray) of adhered MDMs stained for F-actin (A), β-tubulin (B), acetylated α-tubulin (C) and neutral lipids (D). Nuclei (blue) are visualized by Hoechst 33258. Data are expressed as the mean of total fluorescence intensity in each MDM morphotype (at least three fields, 400× magnification, were analyzed) and derive from three (β-tubulin) and five (F-actin, acetylated α-tubulin, neutral lipids) independent cultures obtained from separate donors. *$P < 0.05$.

As it is known that cytoskeleton takes part in the control of lipid handling by macrophages (Tabas et al., 1994), we determined the lipid content of MDM morphotypes. A significantly higher Nile Red staining was found in round MDMs, which also exhibited cytoplasmatic structures resembling lipid droplets (Fig. 2D).

Respiratory burst

The production of superoxide anion was detected by means of MDM ability either to reduce NBT or to oxidize hydroethidium. Spindle MDMs showed a superior efficiency in reducing NBT, detected by formazan deposition (Fig. 3A). In addition, the nuclear ethidium fluorescence intensity was >2 times in spindle than in round MDMs (Fig. 3B). When MDMs were exposed to PMA, which up-regulates NADPH oxidase in differentiating monocytes (Barbieri et al., 2003), fluorescence intensity markedly increased in both morphotypes and became comparable between spindle and round MDMs (Fig. 3C).

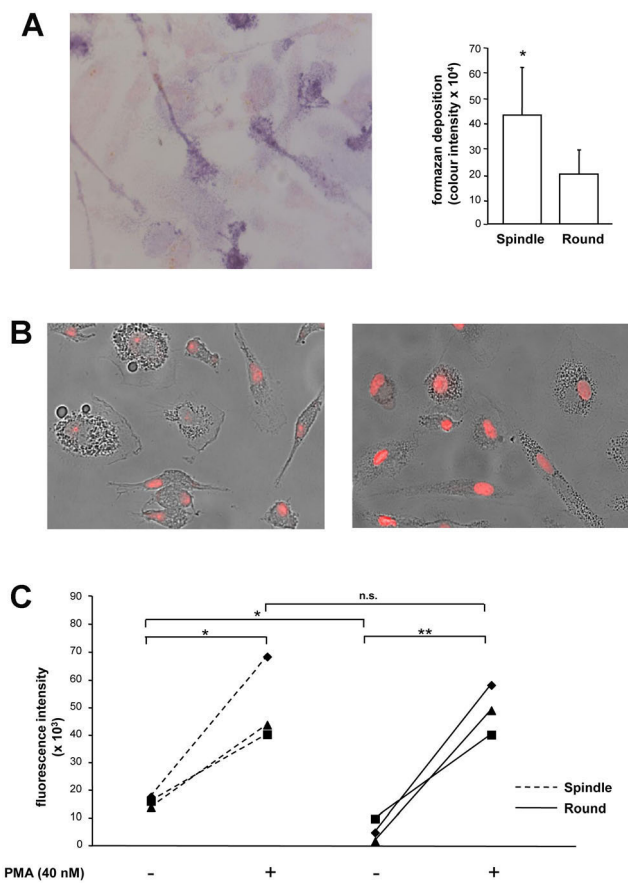

Fig. 3. Superoxide anion generation. Representative cytochemistry (400× magnification) and quantitative image analyses of adhered resting MDMs exposed to nitroblue tetrazolium for 20 min. Formazan deposition, consequent to intracellular superoxide anion generation, is visualized as blue/violet crystals (A). Representative image (B) and quantitative image analyses (C) of MDMs, either in resting condition (B, left) or exposed to PMA (40 nM, 2 h) (B, right). The red fluorescent product that derives from the reaction of DHE with superoxide anion is localized into nuclei. Data are expressed as the mean of total color/fluorescence intensity in each MDM morphotype (at least three fields, 400× magnification, were analyzed) and derive from five (formazan deposition) and three (DHE oxidation) independent cultures obtained from separate donors. *$P < 0.05$, **$P < 0.02$.

Endocytotic profile

Macrophages take up antigens via endocytosis, either receptor-mediated (mostly C-type lectin receptors) or in fluid-phase (e.g., macropinocytosis) (Kerr and Teasdale, 2009; Wang and Chandawarkar, 2010). The uptake of Dextran^{FITC} (40 kDa) was comparable between round and spindle MDMs (Fig. 4A), whereas the uptake of Lucifer Yellow that occurs via macropinocytosis (Krysko et al., 2006) was significantly more efficient in round MDMs (Fig. 4B).

Binding/uptake of apoptotic Jurkat T-cells

The apoptosis of Jurkat T-cells induced by etoposide was barely detectable at 2 h (5.4 ± 1.3% apoptotic cells, n = 6) and increased at 20 h (60.3 ± 3.6% apoptotic cells, n = 3). Exposure of MDMs to "early" apoptotic Jurkat for 1 h (MDMs/apoptotic cell ratio ~2:1) resulted in a higher capacity of round MDMs to bind/uptake cells, as shown by the appearance of CFSE-positive apoptotic material (Fig. 5A). Time-course experiments documented that this superior capacity was maintained in time, for at least 2 h (Fig. 5B). Conversely, when MDMs were exposed to "late" apoptotic Jurkat, whose internalization is receptor-mediated (Reefman et al., 2007), the extent of binding/uptake did not differ between the two morphotypes (data not shown).

CD163 and IL-10 expression

Apoptotic cell clearance is a non-inflammatory process (Fadok et al., 1998) that triggers tolerogenic responses in the adaptive immune system (Savill et al., 2002). Based on this, we sought to determine whether the two morphotypes were characterized by a distinct expression pattern of the haptoglobin/hemoglobin

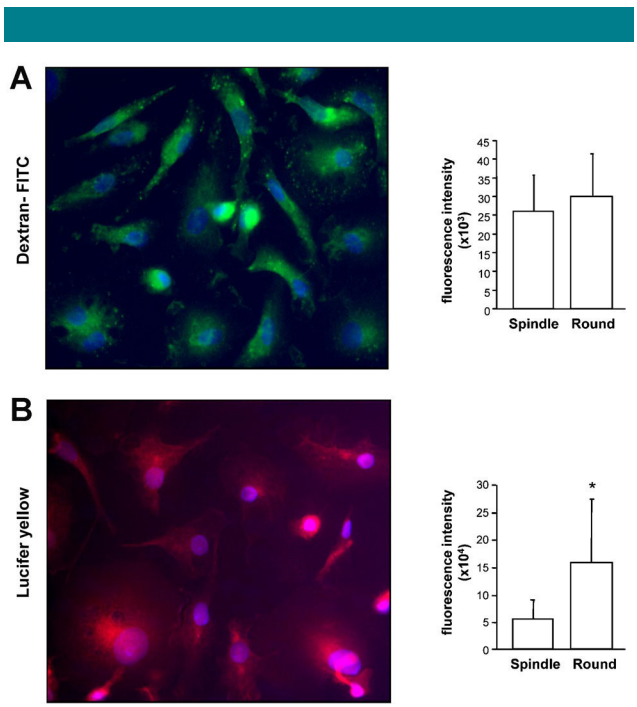

Fig. 4. Lectin-mediated endocytosis and macropinocytosis. Representative immunofluorescence images (400× magnification) and quantitative image analyses of adhered MDMs incubated for 2 h with Dextran^{FITC} (A) or with Lucifer Yellow (B) (1 mg/ml both). Data are expressed as the mean of total intracellular fluorescence intensity in each MDM morphotype (at least three fields, 400× magnification, were analyzed) and derive from six independent cultures obtained from separate donors. *$P < 0.05$.

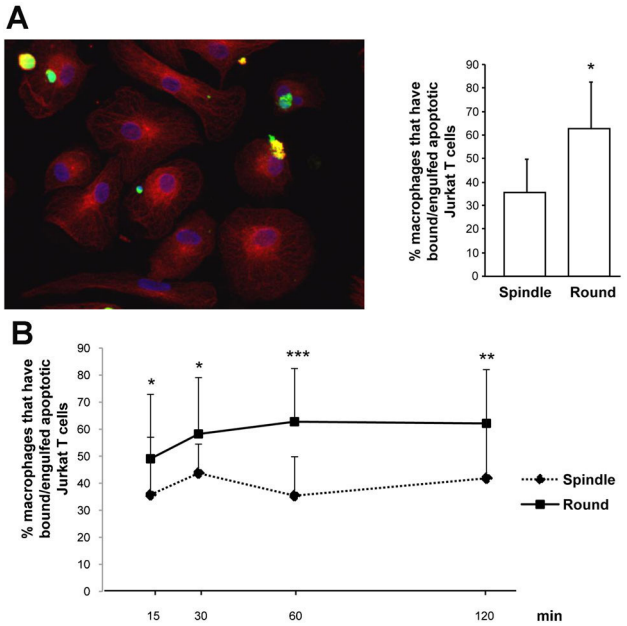

Fig. 5. Binding/uptake of apoptotic Jurkat T-cells. Representative immunofluorescence images (magnification 400×) and quantitative image analyses of adhered MDMs incubated for 1 h with early apoptotic Jurkat T-cells (CSFE-labeled, yellow/green) and subsequently immunostained for β-tubulin (red) and nucleic acid (blue). The extent of binding/uptake was expressed as the percentage of MDMs that have bound/engulfed apoptotic cells, reported to the total macrophage number of each morphotype (at least three fields, 400× magnification, were analyzed) (A). Time-dependent binding/uptake of early apoptotic Jurkat T-cells. The extent of binding/uptake was expressed as above (B). Data are expressed as the mean of total fluorescence intensity in each MDM morphotype (at least three fields, 400× magnification, were analyzed). All data shown derive from seven independent cultures obtained from separate donors. $^{*}P < 0.05$, $^{**}P < 0.02$, $^{***}P < 0.001$.

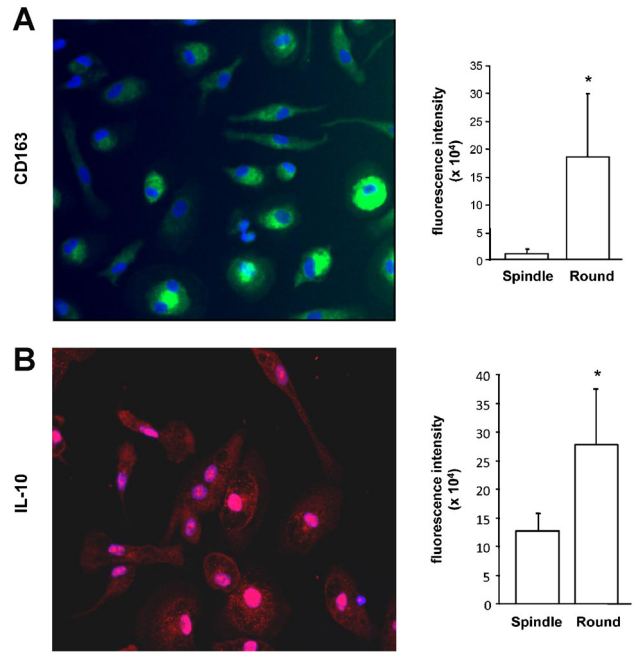

Fig. 6. CD163 and IL-10 expression. Representative immunofluorescence images (magnification 400×) and quantitative image analysis of adhered MDMs stained for CD163 (green) (A) and IL-10 (red, punctuate) (B). Nuclei are visualized in blue. Data are expressed as the mean of total fluorescence intensity in each MDM morphotype (at least three fields, 400× magnification, were analyzed). All data shown derive from six independent cultures obtained from separate donors. $^{*}P < 0.05$.

scavenger receptor CD163 and of IL-10, both associated with a non-inflammatory and anti-atherogenic phenotype (Philippidis et al., 2004; Guetta et al., 2007; Couper et al., 2008; McLaren et al., 2011). Results indicate that CD163 and IL-10 staining were more intense in round-shaped MDMs (Fig. 6A,B), a feature that goes in parallel with their higher capacity to clear "early" apoptotic cells, as reported (Xu et al., 2006).

Transcriptional cytokine/chemokine profile

To compare the cytokine/chemokine transcriptional profile of the dominant MDM morphotypes, we performed a qRT-PCR analysis on amplified RNA from matched round and spindle MDMs of six independent preparations. We identified 41 cytokine and/or chemokine genes expressed by either morphotypes, 11 of which showed a significant differential expression (Table 1). Round MDMs showed overexpression of eight transcripts, among which the gene that encodes for the cytokines IL-10 ($P = 0.003$), IL-24 ($P = 0.013$), and IL-27 ($P = 0.024$). TGFβ2 was expressed only by round and not by spindle MDMs ($P = 0.007$). By contrast, genes overexpressed in spindle MDMs encode for the pro-inflammatory chemokines CCL24 ($P = 0.010$) and CCL18 ($P = 0.019$). Other genes showed an apparent high mean fold difference between spindle and round MDMs, such as CCL2 and CCL8 (2.10- and 4.94-fold increase, respectively) but this did not reach statistical significance. Since RNA quality and internal controls were similar for the six donors, the lack of significant difference in relative gene expression probably reflects normal donor-to-donor variability and/or a higher degree of heterogeneity within the spindle morphotype. Unsupervised clustering analysis of the differentially expressed genes correctly discriminates between round and spindle-shaped MDMs from the six samples (Fig. 7), separating them almost completely in two clusters. This suggests that the two morphotypes bear a different transcriptional signature.

Discussion

Increasing evidence strengthens the consensus that macrophages comprise heterogeneous populations: several co-existing subtypes with diverse, even opposing specialties have been described in inflammation, tumor biology and atherogenesis (Mosser and Edwards, 2008).

Tumor microenvironments contain functionally distinct subsets of monocyte-derived macrophages that orchestrate the activity of the tumor protection system (Movahedi et al., 2010; Heusinkveld et al., 2011). In addition, upregulation of specific sets of genes in response to plaque lipids has been recently reported in macrophages, suggesting that different stages in the progression of atherosclerosis are associated with the presence of distinct subtypes (Adamson and Leitinger, 2011; Pello et al., 2011).

Protocols commonly used to obtain MDMs employ monocytic cell lines exposed to agents that promote differentiation or make use of monocytes exposed to CSFs and/or cytokines. The former are advantageous in terms of cell availability and handling, but data cannot be easily extrapolated

TABLE 1. Comparison of cytokine and chemokine expression in round versus spindle-shaped MDM

Symbol	Gene name	Round[a]	Spindle[a]	Fold difference	*P*-value[b]	FDR[c]
TGFB2	**Transforming growth factor β2**	**0.82 ± 0.73**	**0.04 ± 0.06**	**18.47**	**0.007**	**0.13**
CX3CL1	**Chemokine (C-X3-C motif) ligand 1**	**2.01 ± 0.96**	**0.41 ± 0.27**	**4.89**	**0.013**	**0.13**
IL24	**Interleukin 24**	**2.71 ± 1.79**	**0.66 ± 0.39**	**4.13**	**0.013**	**0.11**
CCL3	Chemokine (C–C motif) ligand 3	1.80 ± 1.80	0.44 ± 0.32	4.13	0.058	0.20
CCL22	**Chemokine (C-C motif) ligand 22**	**1.66 ± 0.70**	**0.50 ± 0.53**	**3.31**	**0.017**	**0.12**
IL27	**Interleukin 27**	**1.42 ± 1.20**	**0.45 ± 0.43**	**3.14**	**0.024**	**0.11**
IL10	**Interleukin 10**	**1.81 ± 1.23**	**0.84 ± 0.71**	**2.14**	**0.003**	**0.11**
CSF1	**Colony stimulating factor 1 (macrophage)**	**1.89 ± 0.67**	**0.94 ± 0.83**	**2.00**	**0.043**	**0.16**
GPI	**Glucose-6 phosphate isomerase**	**2.83 ± 1.68**	**1.64 ± 0.44**	**1.73**	**0.028**	**0.11**
TNFSF13B	Tumor necrosis factor (ligand) superfamily, member 13b	2.68 ± 2.33	1.61 ± 0.78	1.66	0.518	0.71
CXCL1	Chemokine (C–X–C motif) ligand 1	1.12 ± 1.02	0.74 ± 0.75	1.51	0.290	0.46
CCL1	Chemokine (C–C motif) ligand 1	1.79 ± 1.49	1.20 ± 0.88	1.50	0.283	0.48
MIF	Macrophage migration inhibitory factor	2.40 ± 1.43	1.66 ± 0.59	1.44	0.136	0.33
IL1RN	**Interleukin 1 receptor antagonist**	**1.90 ± 0.39**	**1.39 ± 0.56**	**1.37**	**0.023**	**0.12**
VEGFA	Vascular endothelial growth factor A	1.51 ± 1.05	1.11 ± 0.74	1.36	0.599	0.77
SPP1	Secreted phosphoprotein 1	1.47 ± 0.75	1.12 ± 0.49	1.31	0.120	0.38
IL16	Interleukin 16	0.96 ± 0.60	0.77 ± 0.49	1.25	0.403	0.61
CXCL16	Chemokine (C–X–C motif) ligand 16	1.53 ± 0.53	1.28 ± 0.31	1.20	0.166	0.38
IL8	Interleukin 8	0.98 ± 0.90	0.83 ± 0.90	1.18	0.908	1.01
C5	Complement component 5	0.95 ± 0.29	0.84 ± 0.30	1.13	0.560	0.74
CCL20	Chemokine (C–C motif) ligand 20	0.67 ± 0.38	0.64 ± 0.29	1.06	0.672	0.83
TNFSF10	Tumor necrosis factor (ligand) superfamily, member 10	0.67 ± 0.58	0.64 ± 0.74	1.06	0.135	0.35
IL15	Interleukin 15	1.34 ± 0.55	1.35 ± 0.69	−1.01	0.847	0.96
IL23A	Interleukin 23α subunit p19	1.05 ± 0.55	1.06 ± 0.69	−1.01	0.927	0.97
IL1A	Interleukin 1α	0.27 ± 0.33	0.28 ± 0.43	−1.02	0.128	0.35
IL18	Interleukin 18 (interferon-γ-inducing factor)	1.28 ± 1.22	1.33 ± 0.91	−1.04	0.431	0.63
CCL17	Chemokine (C–C motif) ligand 17	0.46 ± 0.32	0.51 ± 0.97	−1.09	0.182	0.39
LIF	Leukemia inhibitory factor	0.73 ± 0.32	0.92 ± 0.78	−1.26	0.909	0.98
OSM	Oncostatin M	0.62 ± 0.51	0.80 ± 0.66	−1.29	0.927	0.95
BMP6	Bone morphogenetic protein 6	0.48 ± 0.47	0.66 ± 0.95	−1.39	0.733	0.88
LTB	Lymphotoxin β (TNF superfamily, member 3)	0.84 ± 0.35	1.22 ± 0.76	−1.45	0.128	0.37
CXCL2	Chemokine (C–X–C motif) ligand 2	0.42 ± 0.38	0.64 ± 0.46	−1.51	0.229	0.47
CCL5	Chemokine (C–C motif) ligand 5	0.40 ± 0.29	0.64 ± 0.91	−1.61	0.791	0.93
TNF	Tumor necrosis factor	0.48 ± 0.34	0.87 ± 0.95	−1.82	0.261	0.49
CCL7	Chemokine (C–C motif) ligand 7	0.41 ± 0.29	0.77 ± 0.70	−1.87	0.230	0.45
IL1B	Interleukin 1β	0.56 ± 0.41	1.06 ± 0.86	−1.89	0.267	0.48
CCL2	Chemokine (C–C motif) ligand 2	0.43 ± 0.31	0.91 ± 1.02	−2.10	0.514	0.73
CXCL5	Chemokine (C–X–C motif) ligand 5	0.19 ± 0.29	0.46 ± 0.64	−2.48	0.930	0.93
CCL18	**Chemokine (C–C motif) ligand 18**	**0.20 ± 0.19**	**0.65 ± 0.42**	**−3.33**	**0.019**	**0.11**
CCL8	Chemokine (C–C motif) ligand 8	0.17 ± 0.11	0.88 ± 0.95	−4.94	0.288	0.47
CCL24	**Chemokine (C–C motif) ligand 24**	**0.10 ± 0.20**	**0.71 ± 1.16**	**−7.10**	**0.010**	**0.14**

Bold, significantly different genes.
[a]Mean ± SD of normalized mRNA expression levels.
[b]Nominal *P*-value.
[c]FDR, false discovery rate.

to tissue macrophages because of the marked impact of the kind of differentiation treatment and duration on gene transcription (Kohro et al., 2004; Daigneault et al., 2010). The latter allow the differentiation of macrophages with distinct profiles according to the type of CSF added to the culture medium (Akagawa, 2002). This approach has permitted the disclosure of distinct macrophage functional programs, but the culture condition does not mirror the tissue environment-specific signals and hence it is questionable whether deductions drawn may be appropriate for tissue macrophages.

In this study, we have characterized two dominant MDM morphotypes, different in dimensions and shape (round and spindle), originated by spontaneous differentiation of human monocytes cultured for 7 days in autologous serum to preserve the individual traits of each donor. In addition, monocytes were cultured in the presence of autologous, spontaneously adherent lymphocytes, which may possibly drive monocyte differentiation by either direct cell–cell interaction or by soluble paracrine mechanisms.

The two MDM populations, besides morphology, exhibit distinct traits in terms of cytoskeleton architecture, lipid content, respiratory burst efficiency, endocytosis, CD163 expression, and transcriptional cytokine/chemokine profile.

Round MDMs show a peculiar distribution of F-actin that is aggregated in dense perinuclear core. Interestingly, recent data indicate that actin undergoes nuclear translocation and participates to transcriptional regulation in HL-60 differentiated towards macrophages (Xu et al., 2010). The composition of microtubule network is also diverse, with the presence of stable and long-lived microtubules that is more pronounced in round MDMs. Taken together, our data indicate that macrophage morphology is strictly related to distinct cytoskeleton organization patterns. In this respect, it has been reported that human macrophages cultured with granulocyte/monocyte-CSF (GM-CSF) or monocyte-CSF (M-CSF) acquire different morphologies, elongated/motile, and flatter, respectively (De Nichilo and Burns, 1993). Cytoskeleton plays a pivotal role in atherogenic lipoprotein handling processes by macrophages (Tabas et al., 1994). In particular, cytoskeleton controls the uptake of oxidized LDL mediated by the scavenger receptor CD36 (Jaqaman et al., 2011) and, in turn, macrophage exposure to oxidized LDL results in robust actin polymerization (Miller et al., 2003). In our preparations, the round morphotype is characterized by higher levels of neutral lipids that are concomitant with enhanced microtubule stabilization, a feature compatible with a scarcely motile phenotype when compared to that of elongated cells (van Gils et al., 2012). The observed association between cytoskeleton architecture and lipid accumulation supports the postulate that macrophage-derived foam cells lose the ability to migrate after lipid loading and thus accumulate in the arterial wall (Wintergerst et al., 1998). Consistently, lipid loading impairs actin distribution, locomotor forces, and motility in J774 macrophages (Zerbinatti and Gore, 2003; Adorni et al., 2011).

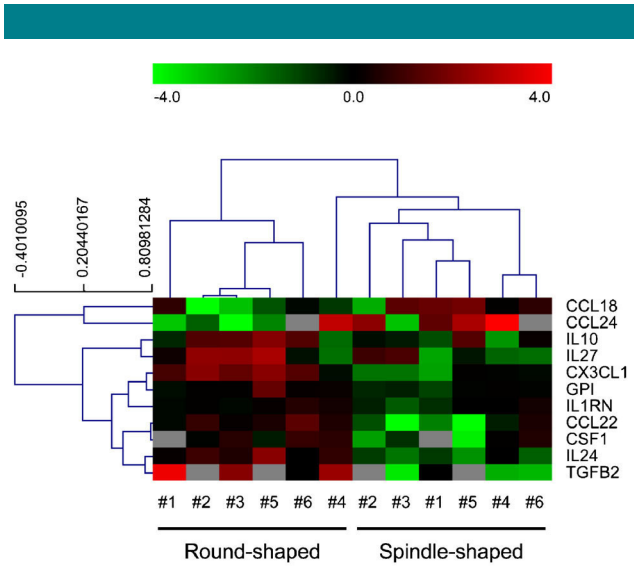

Fig. 7. Unsupervised hierarchical clustering of differentially expressed cytokine/chemokine genes. Expression data were collected from the corresponding profiling experiments, performed on amplified RNA from six independent MDM preparations. Normalized, log_2 transformed, median centered gene expression values are represented with a green-to-red color scale (green indicating below and red above the median value). Sample and genes are clustered by uncentered Pearson's correlation and average linkage.

Round, lipid-enriched MDMs are less efficient in producing superoxide anion. In line with this, a defective respiratory burst has been shown in a granuloma-specific macrophage population characterized by high lipid content (Peyron et al., 2008). The different capacity of round and spindle MDMs to produce superoxide anion was abolished by exposure to PMA. This finding indicates that, despite initial difference in phenotype, MDMs can readily shift their functional properties upon adequate challenge.

The two populations exhibit a comparable capacity for receptor-mediated endocytosis, whereas round MDMs show a superior macropinocytosis. A similar behavior has been reported in macrophages differentiated from peripheral blood monocytes in the presence of GM-CSF or M-CSF to obtain classically or alternatively activated MDMs: dextran^{FITC} uptake by M1 and M2 was comparable, whereas that of Lucifer Yellow was preferential for M2 (Xu et al., 2006). In addition, round MDMs show an almost twofold higher capacity to bind/uptake early apoptotic Jurkat T-cells. Thus, a relationship among efficiency of macropinocytosis, lipid enrichment, and cytoskeleton organization may be delineated. It has been reported that macropinocytosis of native LDL occurs through actin rearrangement (Kruth et al., 2005) and that microtubule integrity is required for an efficient phagocytosis in RAW 264.7 macrophages (Khandani et al., 2007). The higher F-actin labeling coupled with the increased subset of stable microtubules observed in round-shaped MDMs is well in line with these observations.

The binding, uptake, and clearance of apoptotic cells, termed efferocytosis, is a silent process in that the production of pro-inflammatory mediators is prevented (Fadok et al., 1998). The anti-inflammatory program activated by efferocytosis has been evidenced either in alveolar macrophages (Medeiros et al., 2009) or in polarized M2 phenotype, which preferentially binds and ingests early apoptotic cells and produces high levels of IL-10 (Xu et al., 2006). In our cultures, round MDMs exhibit an anti-inflammatory profile, outlined by a more efficient binding/uptake of apoptotic cells in parallel with an increased expression of the non-inflammatory haptoglobin/hemoglobin receptor CD163. This profile is identical to that described in human peritoneal macrophages (Xu et al., 2007). In addition, the increased levels of IL-10 (both mRNA and protein) in round MDMs reinforce the evidence of their non-inflammatory phenotype. Of note, the concerted action of IL-10 and CD163 contributes to the generation of an immunosuppressive environment within a tumor (Sierra-Filardi et al., 2010).

The cytokine/chemokine expression of the two morphotypes indicates distinct transcriptional programs that appear consistent with the profile delineated above: a non-inflammatory and reparative phenotype (round MDMs) and a pro-inflammatory phenotype that advise a paracrine cross-talk with other cells in primary immune responses and allergic inflammation (spindle MDMs). Indeed, round MDMs overexpress IL-10 and TGFβ2. In particular, the latter stimulates the proliferation of hematopoietic precursors in a paracrine way (Shah et al., 2011) and possesses wound repair capacity (Lagord et al., 2002). By contrast, genes that are highly expressed in spindle MDMs encode for the pro-inflammatory chemokines CCL24 and CCL18. CCL24 is involved in macrophage driven activation of T lymphocytes (Ancuta et al., 2006) and eosinophil recruitment in allergic inflammation (Luster, 2001), whereas CCL18 contributes to the physiological homing of lymphocytes and sustains inflammation by attracting various leukocyte populations (Schutyser et al., 2005). Of interest, CCL18 expression has been reported in a subset of macrophages in human carotid plaques (Hagg et al., 2009).

In conclusion, we have characterized two distinct, predominant macrophage phenotypes that occur in the same MDM culture following 7 days differentiation in the presence of autologous serum. Notably, these phenotypes exhibit a number of features that resemble M1 and M2 profile. In particular, round MDMs show functional traits reminiscent of anti-inflammatory M2, as evidenced by their increased efficiency to bind and uptake apoptotic cells that goes in parallel with increased CD163 expression and IL-10 levels. Conversely, the higher capacity of the spindle morphotype to produce superoxide anion coupled with increased mRNA levels of the proinflammatory chemokines CCL18 and CCL24 is suggestive of a classical activated phenotype.

Since tissue macrophages are difficult to obtain and handle, this experimental model may be used as a "surrogate" to study them. The main limitations of this model are (i) the lack of cell turnover, (ii) the absence of tissue-specific matrix proteins, and (iii) a "tailored" lifespan, which are all critical in shaping tissue macrophage behavior. Nevertheless, the proposed model of blood monocyte differentiation in vitro may be valuable to address the impact of tissue macrophage heterogeneity on diseases regulated by these immune cells, also in view of therapeutic manipulations.

Literature Cited

Adamson S, Leitinger N. 2011. Phenotypic modulation of macrophages in response to plaque lipids. Curr Opin Lipidol 22:335–342.

Adorni MP, Favari E, Ronda N, Granata A, Bellosta S, Arnaboldi L, Corsini A, Gatti R, Bernini F. 2011. Free cholesterol alters macrophage morphology and mobility by an ABCA1 dependent mechanism. Atherosclerosis 215:70–76.

Akagawa KS. 2002. Functional heterogeneity of colony-stimulating factor-induced human monocyte-derived macrophages. Int J Hematol 76:27–34.

Ancuta P, Wang J, Gabuzda D. 2006. CD16+ monocytes produce IL-6, CCL2, and matrix metalloproteinase-9 upon interaction with CX3CL1-expressing endothelial cells. J Leukoc Biol 80:1156–1164.

Andersen CL, Jensen JL, Orntoft TF. 2004. Normalization of real-time quantitative reverse transcription-PCR data: A model-based variance estimation approach to identify genes suited for normalization, applied to bladder and colon cancer data sets. Cancer Res 64:5245–5250.

Barbieri SS, Eligini S, Brambilla M, Tremoli E, Colli S. 2003. Reactive oxygen species mediate cyclooxygenase-2 induction during monocyte to macrophage differentiation: Critical role of NADPH oxidase. Cardiovasc Res 60:187–197.

Benoit M, Desnues B, Mege JL. 2008. Macrophage polarization in bacterial infections. J Immunol 181:3733–3739.
Colli S, Lalli M, Rise P, Mussoni L, Eligini S, Galli C, Tremoli E. 1999. Increased thrombogenic potential of human monocyte-derived macrophages spontaneously transformed into foam cells. Thromb Haemost 81:576–581.
Couper KN, Blount DG, Riley EM. 2008. IL-10: The master regulator of immunity to infection. J Immunol 180:5771–5777.
Daigneault M, Preston JA, Marriott HM, Whyte MK, Dockrell DH. 2010. The identification of markers of macrophage differentiation in PMA-stimulated THP-1 cells and monocyte-derived macrophages. PLoS ONE 5:e8668.
De Nichilo MO, Burns GF. 1993. Granulocyte-macrophage and macrophage colony-stimulating factors differentially regulate alpha v integrin expression on cultured human macrophages. Proc Natl Acad Sci USA 90:2517–2521.
Fadok VA, Bratton DL, Konowal A, Freed PW, Westcott JY, Henson PM. 1998. Macrophages that have ingested apoptotic cells in vitro inhibit proinflammatory cytokine production through autocrine/paracrine mechanisms involving TGF-beta, PGE2, and PAF. J Clin Invest 101:890–898.
Fujita E, Shimizu A, Masuda Y, Kuwahara N, Arai T, Nagasaka S, Aki K, Mii A, Natori Y, Iino Y, Katayama Y, Fukuda Y. 2010. Statin attenuates experimental anti-glomerular basement membrane glomerulonephritis together with the augmentation of alternatively activated macrophages. Am J Pathol 177:1143–1154.
Gordon S, Taylor PR. 2005. Monocyte and macrophage heterogeneity. Nat Rev Immunol 5:953–964.
Guetta J, Strauss M, Levy NS, Fahoum L, Levy AP. 2007. Haptoglobin genotype modulates the balance of Th1/Th2 cytokines produced by macrophages exposed to free hemoglobin. Atherosclerosis 191:48–53.
Hagg DA, Olson FJ, Kjelldahl J, Jernas M, Thelle DS, Carlsson LM, Fagerberg B, Svensson PA. 2009. Expression of chemokine (C-C motif) ligand 18 in human macrophages and atherosclerotic plaques. Atherosclerosis 204:e15–e20.
Heusinkveld M, de Vos van Steenwijk PJ, Goedemans R, Ramwadhdoebe TH, Gorter A, Welters MJ, van Hall T, van der Burg SH. 2011. M2 macrophages induced by prostaglandin E2 and IL-6 from cervical carcinoma are switched to activated M1 macrophages by CD4+ Th1 cells. J Immunol 187:1157–1165.
Jaqaman K, Kuwata H, Touret N, Collins R, Trimble WS, Danuser G, Grinstein S. 2011. Cytoskeletal control of CD36 diffusion promotes its receptor and signaling function. Cell 146:593–606.
Johnson JL, Newby AC. 2009. Macrophage heterogeneity in atherosclerotic plaques. Curr Opin Lipidol 20:370–378.
Kerr MC, Teasdale RD. 2009. Defining macropinocytosis. Traffic 10:364–371.
Khandani A, Eng E, Jongstra-Bilen J, Schreiber AD, Douda D, Samavarchi-Tehrani P, Harrison RE. 2007. Microtubules regulate PI-3K activity and recruitment to the phagocytic cup during Fcgamma receptor-mediated phagocytosis in nonelicited macrophages. J Leukoc Biol 82:417–428.
Kohro T, Tanaka T, Murakami T, Wada Y, Aburatani H, Hamakubo T, Kodama T. 2004. A comparison of differences in the gene expression profiles of phorbol 12-myristate 13-acetate differentiated THP-1 cells and human monocyte-derived macrophage. J Atheroscler Thromb 11:88–97.
Kruth HS, Jones NL, Huang W, Zhao B, Ishii I, Chang J, Combs CA, Malide D, Zhang WY. 2005. Macropinocytosis is the endocytic pathway that mediates macrophage foam cell formation with native low density lipoprotein. J Biol Chem 280:2352–2360.
Krysko DV, Denecker G, Festjens N, Gabriels S, Parthoens E, D'Herde K, Vandenabeele P. 2006. Macrophages use different internalization mechanisms to clear apoptotic and necrotic cells. Cell Death Differ 13:2011–2022.
Lagord C, Berry M, Logan A. 2002. Expression of TGFbeta2 but not TGFbeta1 correlates with the deposition of scar tissue in the lesioned spinal cord. Mol Cell Neurosci 20:69–92.
Lambrecht BN. 2006. Alveolar macrophage in the driver's seat. Immunity 24:366–368.
Ley K, Miller YI, Hedrick CC. 2011. Monocyte and macrophage dynamics during atherogenesis. Arterioscler Thromb Vasc Biol 31:1506–1516.
Lumeng CN, Bodzin JL, Saltiel AR. 2007. Obesity induces a phenotypic switch in adipose tissue macrophage polarization. J Clin Invest 117:175–184.
Luster AD. 2001. Antichemokine immunotherapy for allergic diseases. Curr Opin Allergy Clin Immunol 1:561–567.
Mantovani A, Sozzani S, Locati M, Allavena P, Sica A. 2002. Macrophage polarization: Tumor-associated macrophages as a paradigm for polarized M2 mononuclear phagocytes. Trends Immunol 23:549–555.
Mantovani A, Sica A, Sozzani S, Allavena P, Vecchi A, Locati M. 2004. The chemokine system in diverse forms of macrophage activation and polarization. Trends Immunol 25:677–686.
McLaren JE, Michael DR, Ashlin TG, Ramji DP. 2011. Cytokines, macrophage lipid metabolism and foam cells: Implications for cardiovascular disease therapy. Prog Lipid Res 50:331–347.
Medeiros AI, Serezani CH, Lee SP, Peters-Golden M. 2009. Efferocytosis impairs pulmonary macrophage and lung antibacterial function via PGE2/EP2 signaling. J Exp Med 206:61–68.
Miller YI, Worrall DS, Funk CD, Feramisco JR, Witztum JL. 2003. Actin polymerization in macrophages in response to oxidized LDL and apoptotic cells: Role of 12/15-lipoxygenase and phosphoinositide 3-kinase. Mol Biol Cell 14:4196–4206.
Mosser DM, Edwards JP. 2008. Exploring the full spectrum of macrophage activation. Nat Rev Immunol 8:958–969.
Movahedi K, Laoui D, Gysemans C, Baeten M, Stange G, Van den Bossche J, Mack M, Pipeleers D, In't Veld P, De Baetselier P, Van Ginderachter JA. 2010. Different tumor microenvironments contain functionally distinct subsets of macrophages derived from Ly6C(high) monocytes. Cancer Res 70:5728–5739.
Murray PJ, Wynn TA. 2011. Protective and pathogenic functions of macrophage subsets. Nat Rev Immunol 11:723–737.
Pello OM, Silvestre C, De Pizzol M, Andres V. 2011. A glimpse on the phenomenon of macrophage polarization during atherosclerosis. Immunobiology 216:1172–1176.
Peyron P, Vaubourgeix J, Poquet Y, Levillain F, Botanch C, Bardou F, Daffe M, Emile JF, Marchou B, Cardona PJ, de Chastellier C, Altare F. 2008. Foamy macrophages from tuberculous patients' granulomas constitute a nutrient-rich reservoir for M. tuberculosis persistence. PLoS Pathog 4:e1000204.
Philippidis P, Mason JC, Evans BJ, Nadra I, Taylor KM, Haskard DO, Landis RC. 2004. Hemoglobin scavenger receptor CD163 mediates interleukin-10 release and heme oxygenase-1 synthesis: Antiinflammatory monocyte-macrophage responses in vitro, in resolving skin blisters in vivo, and after cardiopulmonary bypass surgery. Circ Res 94: 119–126.
Reefman E, Horst G, Nijk MT, Limburg PC, Kallenberg CG, Bijl M. 2007. Opsonization of late apoptotic cells by systemic lupus erythematosus autoantibodies inhibits their uptake via an Fcgamma receptor-dependent mechanism. Arthritis Rheum 56:3399–3411.
Saeed AI, Bhagabati NK, Braisted JC, Liang W, Sharov V, Howe EA, Li J, Thiagarajan M, White JA, Quackenbush J. 2006. TM4 microarray software suite. Methods Enzymol 411: 134–193.
Savill J, Dransfield I, Gregory C, Haslett C. 2002. A blast from the past: Clearance of apoptotic cells regulates immune responses. Nat Rev Immunol 2:965–975.
Schutyser E, Richmond A, Van Damme J. 2005. Involvement of CC chemokine ligand 18 (CCL18) in normal and pathological processes. J Leukoc Biol 78:14–26.
Shah CA, Wang H, Bei L, Platanias LC, Eklund EA. 2011. HoxA10 regulates transcription of the gene encoding transforming growth factor beta2 (TGFbeta2) in myeloid cells. J Biol Chem 286:3161–3176.
Sierra-Filardi E, Vega MA, Sanchez-Mateos P, Corbi AL, Puig-Kroger A. 2010. Heme Oxygenase-1 expression in M-CSF-polarized M2 macrophages contributes to LPS-induced IL-10 release. Immunobiology 215:788–795.
Sindrilaru A, Peters T, Wieschalka S, Baican C, Baican A, Peter H, Hainzl A, Schatz S, Qi Y, Schlecht A, Weiss JM, Wlaschek M, Sunderkotter C, Scharffetter-Kochanek K. 2011. An unrestrained proinflammatory M1 macrophage population induced by iron impairs wound healing in humans and mice. J Clin Invest 121:985–997.
Sutherland MW, Learmonth BA. 1997. The tetrazolium dyes MTS and XTT provide new quantitative assays for superoxide and superoxide dismutase. Free Radic Res 27:283–289.
Tabas I, Zha X, Beatini N, Myers JN, Maxfield FR. 1994. The actin cytoskeleton is important for the stimulation of cholesterol esterification by atherogenic lipoproteins in macrophages. J Biol Chem 269:22547–22556.
Van Gelder RN, von Zastrow ME, Yool A, Dement WC, Barchas JD, Eberwine JH. 1990. Amplified RNA synthesized from limited quantities of heterogeneous cDNA. Proc Natl Acad Sci USA 87:1663–1667.
van Gils JM, Derby MC, Fernandes LR, Ramkhelawon B, Ray TD, Rayner KJ, Parathath S, Distel E, Feig JL, Alvarez-Leite JI, Rayner AJ, McDonald TO, O'Brien KD, Stuart LM, Fisher EA, Lacy-Hulbert A, Moore KJ. 2012. The neuroimmune guidance cue netrin-1 promotes atherosclerosis by inhibiting the emigration of macrophages from plaques. Nat Immunol 13:136–143.
Wang R, Chandawarkar RY. 2010. Phagocytosis of fungal agents and yeast via macrophage cell surface scavenger receptors. J Surg Res 164:e273–e279.
Westermann S, Weber K. 2003. Post-translational modifications regulate microtubule function. Nat Rev Mol Cell Biol 4:938–947.
Wilson HM. 2010. Macrophages heterogeneity in atherosclerosis—Implications for therapy. J Cell Mol Med 14:2055–2065.
Wintergerst ES, Jelk J, Asmis R. 1998. Differential expression of CD14, CD36 and the LDL receptor on human monocyte-derived macrophages. A novel cell culture system to study macrophage differentiation and heterogeneity. Histochem Cell Biol 110:231–241.
Xu W, Roos A, Schlagwein N, Woltman AM, Daha MR, van Kooten C. 2006. IL-10-producing macrophages preferentially clear early apoptotic cells. Blood 107:4930–4937.
Xu W, Schlagwein N, Roos A, van den Berg TK, Daha MR, van Kooten C. 2007. Human peritoneal macrophages show functional characteristics of M-CSF-driven anti-inflammatory type 2 macrophages. Eur J Immunol 37:1594–1599.
Xu YZ, Thuraisingam T, Morais DA, Rola-Pleszczynski M, Radzioch D. 2010. Nuclear translocation of beta-actin is involved in transcriptional regulation during macrophage differentiation of HL-60 cells. Mol Biol Cell 21:811–820.
Zerbinatti CV, Gore RW. 2003. Uptake of modified low-density lipoproteins alters actin distribution and locomotor forces in macrophages. Am J Physiol Cell Physiol 284:C555–C561.
Zielonka J, Vasquez-Vivar J, Kalyanaraman B. 2008. Detection of 2-hydroxyethidium in cellular systems: A unique marker product of superoxide and hydroethidine. Nat Protoc 3:8–21.
Zwadlo G, Brocker EB, von Bassewitz DB, Feige U, Sorg C. 1985. A monoclonal antibody to a differentiation antigen present on mature human macrophages and absent from monocytes. J Immunol 134:1487–1492.